



Cadmium selenide quantum dots: synthesis, characterization, and dye removal ability with UV irradiation

Niyaz Mohammad Mahmoodi^{a,*}, Mina Oveisi^a, Amir Masoud Arabi^b, Behzad Karimi^b

^aDepartment of Environmental Research, Institute for Color Science and Technology, Tehran, Iran, Tel. +98 021 22969771; Fax: +98 021 22947537; emails: mahmoodi@icrc.ac.ir (N.M. Mahmoodi), mina.oveisi@znu.ac.ir (M. Oveisi)

^bDepartment of Inorganic Pigment and Glazes, Institute for Color Science and Technology, Tehran, Iran, Tel. +98 021 22969771; Fax: +98 021 22947537; emails: aarabi@icrc.ac.ir (A.M. Arabi), karimiusb@gmail.com (B. Karimi)

Received 19 March 2015; Accepted 28 July 2015

ABSTRACT

In this study, cadmium selenide quantum dots (CdSe-QD) were synthesized and characterized. Dye removal ability of CdSe-QD with UV irradiation (UV/CdSe-QD) was investigated. The synthesized QD was characterized by X-ray diffraction, transmittance electron microscope, Fourier transformation infrared, dynamic light scattering, atomic force microscopy, UV–visible, and photoluminescence analyses. Basic Violet 16, Basic Blue 41, and Acid Blue 92 were used as model dyes. The effect of CdSe-QD dosage on dye removal in presence of UV irradiation was studied. The obtained results showed that dye removal followed by a first-order kinetic model. It has been found that CdSe-QD has dye removal ability from colored wastewater in the presence of UV irradiation.

Keywords: Synthesis; Characterization; Cadmium selenide; Quantum dots; Dye removal ability

1. Introduction

Textile industry is one of the most complex industries among the manufacturing industries. Various textile chemicals such as wetting agents, dyes, surfactants, fixing agents, softeners, and other additives are used in wet processes such as bleaching, dyeing, and finishing processes. As a result, textile wet processing plants produce highly polluted wastewater. Organic synthetic dyes represent relatively large group of organic chemicals, which are present in practically all spheres of mankind daily life. Dyes are all around us, making our world beautiful, but they may cause contamination and therefore the community has to be

focused on the probable environmental problems originated from dye industries. The manufacturing and the processing of dyes involve handling and production of many organic compounds that are toxic and hazardous to human health. The complete mineralization of organic pollutants and decolorization is the most effective way to diminish their environmental impacts [1–8].

Various methods such as biodegradation, coagulation, adsorption, advanced oxidation process (AOP), and membrane process have been suggested to handle dye removal from water. AOPs mainly involve generation of a very powerful and non-selective oxidizing agent, the hydroxyl radical (OH[•]), for destruction of refractory and hazardous pollutants found in

*Corresponding author.

groundwater, surface water, and industrial wastewater [1].

Several nanomaterials such as carbon nanotube, ferrite nanoparticle, and quantum dots (QDs) were used to remove dyes from wastewater [9–15].

QDs have unique optical and electronic properties such as broad excitation and narrow emission spectra, excellent photochemical stability, high photoluminescence (PL) quantum yields, and size-tunable emission profiles [15].

A literature review showed that dye removal ability of cadmium selenide quantum dots (CdSe-QD) with UV irradiation (UV/CdSe-QD) was not investigated in detail. In this study, CdSe-QD was synthesized and characterized. Dye removal ability of CdSe-QD with UV irradiation was investigated. The synthesized QDs were characterized by X-ray diffraction (XRD), transmittance electron microscope (TEM), Fourier transformation infrared (FTIR), dynamic light scattering system (DLS), atomic force microscopy (AFM), UV–visible, and luminescence analyses. Basic Violet 16 (BV16), Basic Blue 41 (BB41), and Acid Blue 92 (AB92) were used as model dyes.

2. Experimental

2.1. Chemicals

Basic Violet 16 (BV16), Basic Blue 41 (BB41), and Acid Blue 92 (AB92) were used as model dyes and

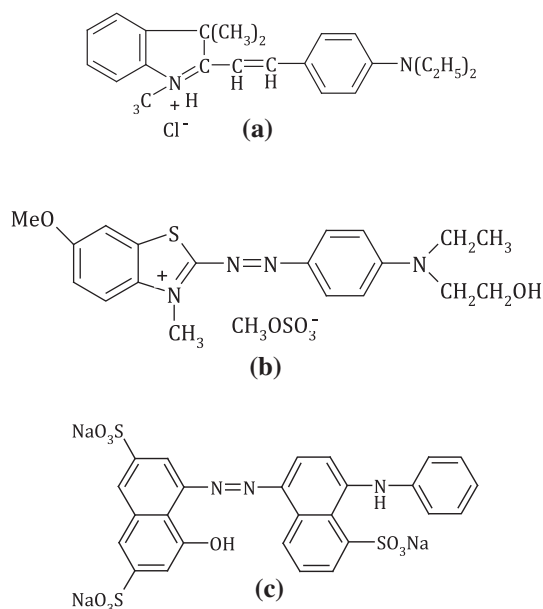


Fig. 1. The chemical structure of dyes (a) BV16, (b) BB41, and (c) AB92.

used without any purification. The chemical structures of dyes were shown in Fig. 1. Cadmium chloride (CdCl₂) was purchased from Sigma-Aldrich. Selenium oxide (SeO₂), sodium borohydride (NaBH₄), and mercaptopropionic acid (MPA) were obtained from Merck Company. All other chemicals were of analytical grade and obtained from Merck (Germany).

2.2. CdSe-QD synthesis characterization

CdSe quantum dots (CdSe-QD) was synthesized by hydrothermal process. 0.056 g SeO₂ and 0.2 g CdCl₂ were mixed with 50 mL of deionized water in a baker and stirred. Then, 0.02 g of NaBH₄ was added for the formation of NaHSe in the hydrothermal process. 0.009 g of MPA as a capping agent was quickly added and pH of the resulted solution was adjusted at 12 by adding 0.1 M NaOH solution. The resulted solution was transferred to 50-mL Teflon lined stainless steel autoclave and put in an oven at 140°C for 2 h. Finally, autoclave was cooled and the resulted QDs were used without further purification.

The structure of CdSe-QD was characterized by XRD pattern (STOE stadi P). Structural studies were done using the QD nanopowder obtained by three times precipitation and redispersion with isopropanol solution, and finally dried in vacuum oven at 70°C. Dried QDs were calcined in a tube furnace at 400°C under N₂ atmosphere. Particle size distribution was measured by DLS system (Malvern, ZEN 3600). Surface image was taken by AFM (Dual scope). Microstructure was investigated by TEM (zeiss EM900). FTIR (Perkin-Elmer Spectrophotometer Spectrum One) was used to determine chemical composition. Optical properties were studied by UV–visible spectrophotometer (Perkin-Elmer lambda 25) and luminescence spectrometer (Perkin-Elmer LS55).

2.3. Dye removal procedure

Experiments were carried out in a batch mode photoreactor. The radiation source was a UV-C lamp (200–280 nm, 9 W Philips). The photocatalytic dye degradation experiments were conducted by mixing CdSe-QD in 800 mL of dye solution (20 mg/L) at room temperature at natural pH (pH 6.5). The solution samples were withdrawn from the reaction medium at regular time intervals. The change on the absorbance at maximum wavelength (λ_{\max}) of dyes (545 nm for BV16, 605 nm for BB41, and 595 nm for AB92) was monitored by UV–vis spectrophotometer (Perkin-Elmer Lambda 25).

3. Results and discussion

3.1. CdSe-QD characterization

Fig. 2 illustrates XRD patterns of dried QDs (before calcination) and QD nanopowder (after calcination). Dried QDs consisted of the broad peaks resulted from very small size QDs [16]. Because of very small size of QDs and bare of passive shells such as ZnS, low temperature calcination of QD nanopowder led to the formation of CdO beside CdSe bulk materials. Sharpening of CdSe peaks after calcination was happened in the same region with the broad peaks of the dried sample and showed the good agreement with wurtzite structure (JCPDS No. 00-008-0459).

DLS experiment was also used to determine the average dynamic size of QDs. As shown in Fig. 3, average size of QD was about 2 nm with narrow size distribution below 5 nm. It can be resulted from the broad peak of dried sample in Fig. 2 and standing the size of particles below 5 nm (Bohr radius of CdSe) that CdSe-QDs were formed.

Although, most of the atoms in the QDs were in the surface and surface area was determined to be high, but measurement of surface area with the dried sample was impossible. As illustrated in Fig. 4, AFM image of dried sample showed the high level of agglomeration.

Fig. 5 illustrates FTIR spectrum of QDs. Some peaks were related to the vibrational modes of the carboxylic group. The narrow and strong peak at $1,396\text{ cm}^{-1}$ and a weak peak at $1,641\text{ cm}^{-1}$ correspond to the COO^- vibrations [17]. C–O stretching is also indicated by the bands ranging from 1,300 to

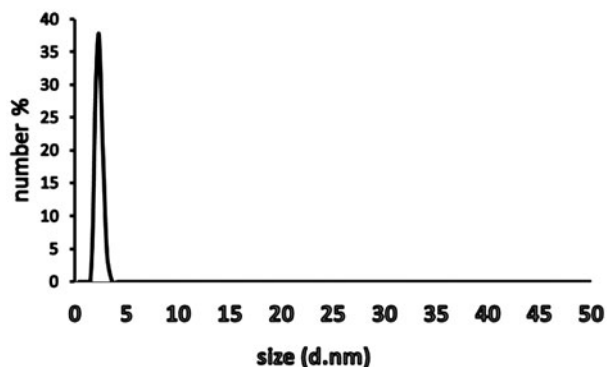


Fig. 3. DLS analysis of CdSe-QDs.

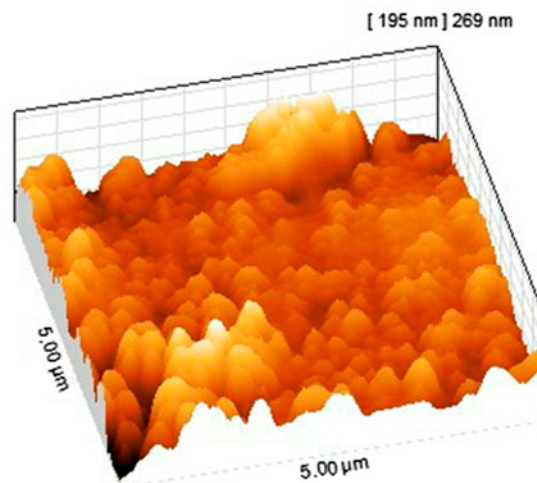


Fig. 4. AFM image of dried CdSe-QDs.

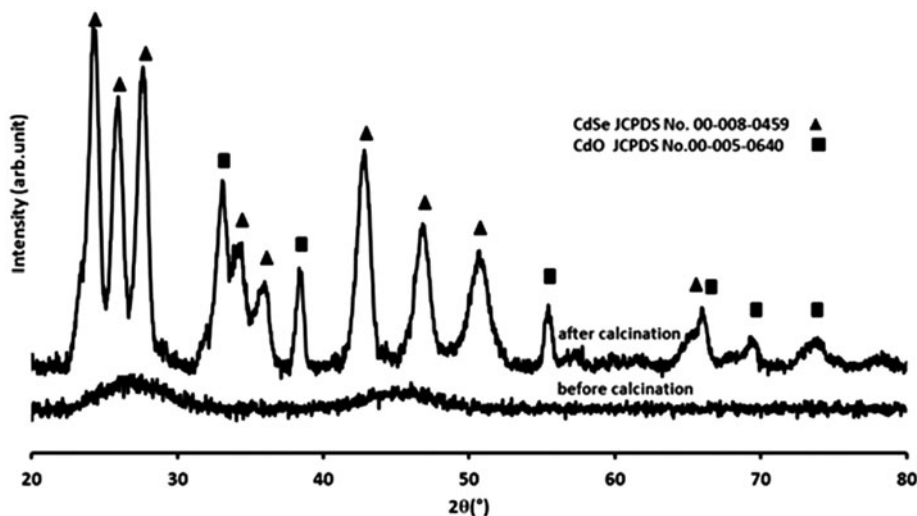


Fig. 2. XRD pattern of dried CdSe-QDs (before and after calcination) at 400°C.

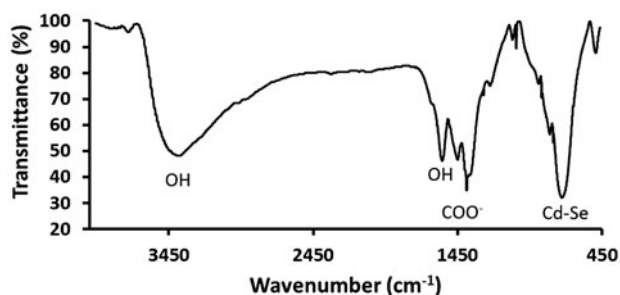


Fig. 5. FTIR spectrum of CdSe-QDs.

$1,000\text{ cm}^{-1}$ [18]. The sharp peak at 722 cm^{-1} can be assigned to Cd–Se band stretching. The peaks at $3,400$ and $1,580\text{ cm}^{-1}$ can be related to OH stretching and bending bands, respectively [19]. FTIR studies revealed the functionalization of CdSe with $-\text{COOH}$ groups [18].

The agglomerates of CdSe-QD are seen in TEM image (Fig. 6). Although, there is not obvious image of QD, but the formation of agglomerates up to 10 nm indicates the formation of particles below Bohr radii and confirms the formation of QD.

UV–visible and PL spectra of CdSe-QD are illustrated in Figs. 7 and 8, respectively. The results showed that the calculated band gap of QDs (inset image of Fig. 7) determined by Tauc method [20] was in good agreement with the change of slope in adsorption curve. This gap data show higher value in comparison with CdSe nanopowders. Moreover, PL spectrum shows blue shift of emission due to quantum confinement effects [17].

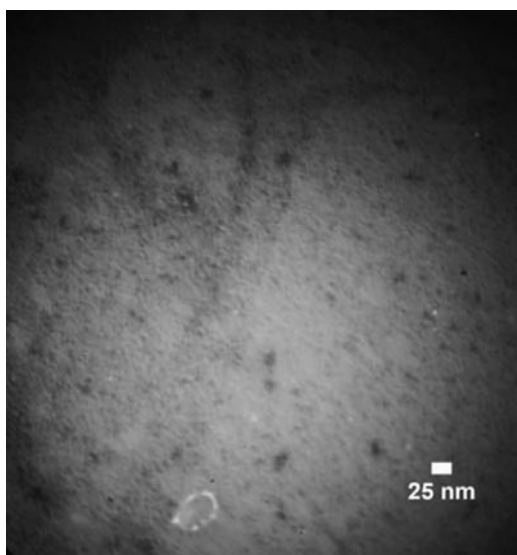


Fig. 6. TEM image of CdSe-QDs.

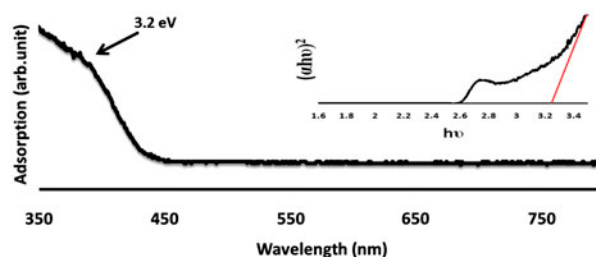


Fig. 7. UV–visible spectrum of CdSe-QD.

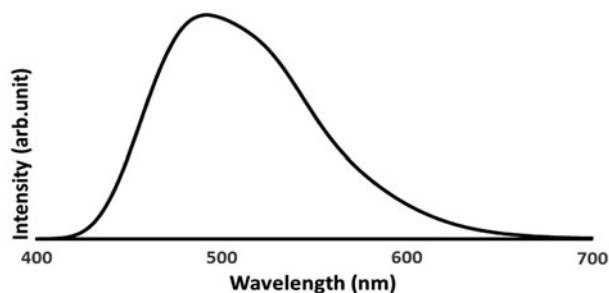


Fig. 8. PL spectrum of CdSe-QD.

3.2. CdSe-QD dye removal ability

Dye removal ability of CdSe-QD without UV irradiation is very low ($<3\%$) (800 mL of dye solution (20 mg/L) and QD: 7.2 mg/L for BV16 and AB92 and 5.2 mg/L for BB41). Thus, dye removal ability of CdSe-QD in the presence of UV irradiation was investigated. The oxidation with UV irradiation in the absence of CdSe-QD is 21 , 11 , and 37% for BV16, BB41, and AB92, respectively (Fig. 9). It is observed that the simultaneous use of CdSe-QD and UV irradiation to a certain extent yielded a significant improvement of dye removal compared to that of the UV irradiation alone (Fig. 9). The synergistic effect of CdSe-QD on UV irradiation was observed because CdSe-QD catalyzes the production of free radicals such as hydroxyl radicals which are very active to degrade pollutants in the aqueous phase.

It has been established that photodegradation of organic matter in solution is initiated by photoexcitation of the semiconductor, followed by the formation of an electron–hole pair on the surface of catalyst. High oxidative potential of the hole (h_{ν}^{+}) in the catalyst permits direct oxidation of the organic matter (dye) to the reactive intermediates. Various reactive radicals can also be formed either by the decomposition of water or by the reaction of the hole with OH^{-} . The hydroxyl radicals are extremely strong, non-selective oxidant ($E_0 = +3.06\text{ V}$) which lead to the partial or

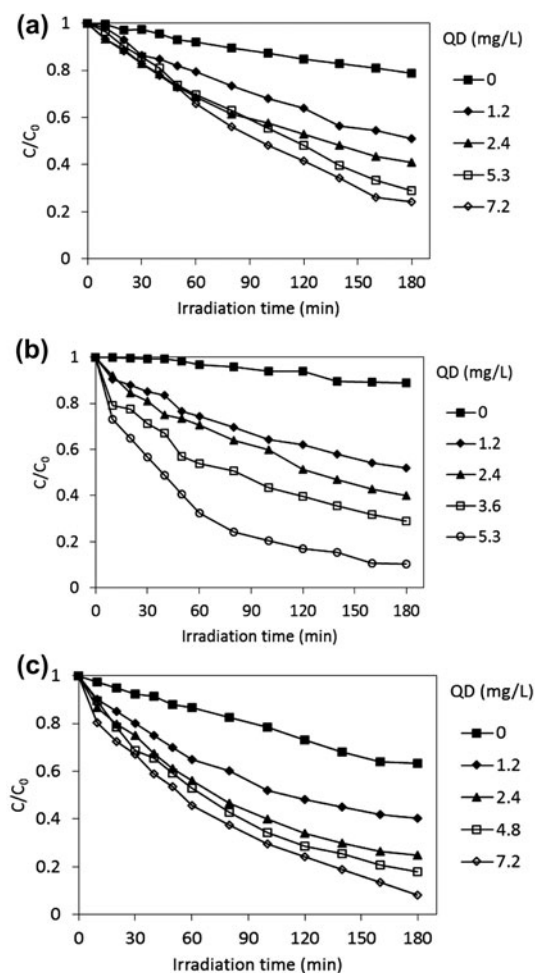


Fig. 9. The effect of CdSe dosage on dye removal by UV/CdSe-QD (a) BV16, (b) BB41, and (c) AB92.

complete mineralization of several organic chemicals. Electron in the conduction band (e_{cb}^-) on the catalyst surface can reduce molecular oxygen to superoxide anion. This radical, in the presence of organic scavengers, may form organic peroxides or hydrogen peroxide. Electrons in the conduction band are also responsible for the production of hydroxyl radicals, species which have been indicated as the primary cause of organic matter mineralization [21].

In this study, various dosages of CdSe-QD were tested on dye removal by UV irradiation (Fig. 9). Results showed that the dye removal efficiency was enhanced by increasing of QD loading. This observation can be explained in terms of availability of active sites on the QD surface and penetration of UV light into the suspension. The total active surface area increases with increasing catalyst dosage. At the same time, due to rising of the suspension turbidity and consequently the scattering effect, UV light penetration

is decreased and hence the photoactivated volume of suspension is declined.

The effect of initial dye concentration was investigated by varying the initial concentration from 20 to 80 mg/L and shown in Table 1. Clearly, the dye concentration affects adsorptive and reactive processes in various manners; first of all, increasing initial dye concentration will enhance the rate of the liquid phase reaction, and surface reaction as well. Meanwhile, the experimental results show that the negative effects of the dye concentration depress the positive ones; the adsorption of dye molecules onto the catalyst surface hinders competitive adsorption of OH^- ions leading to alleviate formation rate of hydroxyl radicals, consequently affects negatively all steps of the mechanism. Furthermore, as the initial dye concentration increases, the path length of photons entering the solution decreases according to the well-known Beer–Lambert law, this means obviously lower photonic absorption on catalyst particles and slower photocatalytic reaction rates.

In order to clarify the changes in the molecular and structural characteristics of the species resultant, the evolution of the UV–vis spectra of each dye solution was recorded as a function of time. The absorption spectrum of dyes is characterized by one main band in the visible region which is associated with the chromophore of the dye molecules. The evolution of the UV–vis spectra during UV/CdSe-QD followed a similar trend for dyes. The spectrum of each dye solution changes along with time by disappearing of the band in the visible region, which determines the color disappearance of the solution [22].

The first-order kinetics of dye removal by UV/CdSe-QD at different CdSe-QD dosages was studied (Table 2). It was possible to fit the curves using first-order model according to the well-known expression [11]:

$$C/C_0 = \exp(-k_1t) \quad (1)$$

Table 1
The effect of initial dye concentration on dye removal by UV/CdSe-QD

Initial dye concentration (mg/L)	Dye removal (%)		
	BV16	BB41	AB92
20	76	90	92
40	61	76	69
60	53	63	55
80	42	55	43

Table 2
The k_1 and R^2 of dye removal by UV/CdSe-QD at different CdSe-QD dosages

Dye	CdSe-QD (mg/L)	k_1 (1/min)	R^2
BV16	0	0.001	0.9949
	1.2	0.004	0.9946
	2.4	0.005	0.9851
	5.3	0.007	0.9876
	7.2	0.008	0.9887
BB41	0	0.001	0.9329
	1.2	0.004	0.9535
	2.4	0.005	0.9823
	3.6	0.007	0.9327
	5.3	0.012	0.9326
AB92	0	0.003	0.9925
	1.2	0.006	0.9349
	2.4	0.009	0.9788
	4.8	0.010	0.9933
	7.2	0.013	0.9862

where C_0 (mg/L) and C (mg/L) are the initial dye concentration and dye concentration at time t , respectively and k_1 (1/min) is the first-order rate constant.

The dye removal rate constant and correlation coefficient (R^2) of dye for the various CdSe-QD dosages are shown in Table 2. The results showed that the kinetics of dye removal using UV/CdSe-QD at different CdSe-QD dosages followed first-order kinetic model.

4. Conclusions

In this study, CdSe-QD was synthesized and characterized. The synthesized QD was characterized by XRD, TEM, FTIR, UV-visible, and luminescence analyses. Dye removal using UV/(CdSe-QD) was investigated. Basic Violet 16, Basic Blue 41, and Acid Blue 92 were used as model dyes. Dye removal efficiency enhanced by increasing QD dosage. The UV-vis spectrum of each dye solution during UV/CdSe-QD changes along with time by the disappearing of the band in the visible region, which determines the color disappearance of the solution. The results showed that the kinetics of dye removal using UV/CdSe-QD followed first-order kinetic model.

References

- [1] I. Arslan-Alaton, I.A. Balcioglu, D.W. Bahnemann, Advanced oxidation of a reactive dyebath effluent: Comparison of O_3 , H_2O_2 /UV-C and TiO_2 /UV-A processes, *Water Res.* 36 (2002) 1143–1154.
- [2] Y. Bulut, H. Aydın, A kinetics and thermodynamics study of methylene blue adsorption on wheat shells, *Desalination* 194 (2006) 259–267.
- [3] N.M. Mahmoodi, S. Khorramfar, F. Najafi, Amine-functionalized silica nanoparticle: Preparation, characterization and anionic dye removal ability, *Desalination* 279 (2011) 61–68.
- [4] N.M. Mahmoodi, B. Hayati, M. Arami, H. Bahrami, Preparation, characterization and dye adsorption properties of biocompatible composite (alginate/titania nanoparticle), *Desalination* 275 (2011) 93–101.
- [5] E. Pajootan, M. Arami, N.M. Mahmoodi, Binary system dye removal by electrocoagulation from synthetic and real colored wastewaters, *J. Taiwan Inst. Chem. Eng.* 43 (2012) 282–290.
- [6] N.M. Mahmoodi, N.Y. Limaee, M. Arami, S. Borhany, M. Mohammad-Taheri, Nanophotocatalysis using nanoparticles of titania: Mineralization and finite element modelling of Solophenyl dye decolorization, *J. Photochem. Photobiol., A: Chem.* 189 (2007) 1–6.
- [7] M.A. Rauf, S.S. Ashraf, Fundamental principles and application of heterogeneous photocatalytic degradation of dyes in solution, *Chem. Eng. J.* 151 (2009) 10–18.
- [8] N.M. Mahmoodi, Magnetic ferrite nanoparticle–alginate composite: Synthesis, characterization and binary system dye removal, *J. Taiwan Inst. Chem. Eng.* 44 (2013) 322–330.
- [9] N.M. Mahmoodi, Manganese ferrite nanoparticle: Synthesis, characterization and photocatalytic dye degradation ability, *Desalin. Water Treat.* 53 (2015) 84–90.
- [10] H.R. Rajabi, M. Farsi, Quantum dot based photocatalytic decolorization as an efficient and green strategy for the removal of anionic dye, *Mater. Sci. Semicond. Process.* 31 (2015) 478–486.
- [11] N.M. Mahmoodi, Synthesis of magnetic carbon nanotube and photocatalytic dye degradation ability, *Environ. Monit. Assess.* 186 (2014) 5595–5604.
- [12] E.K. Goharshadi, M. Hadadian, M. Karimi, H. Azizi-Toupkanloo, Photocatalytic degradation of reactive black 5 azo dye by zinc sulfide quantum dots prepared by a sonochemical method, *Mater. Sci. Semicond. Process.* 16 (2013) 1109–1116.
- [13] N.M. Mahmoodi, Dendrimer functionalized nanoarchitecture: Synthesis and binary system dye removal, *J. Taiwan Inst. Chem. Eng.* 45 (2014) 2008–2020.
- [14] N.M. Mahmoodi, Synthesis of core-shell magnetic adsorbent nanoparticle and selectivity analysis for binary system dye removal, *J. Ind. Eng. Chem.* 20 (2014) 2050–2058.
- [15] X. Luo, B. Guo, L. Wang, F. Deng, R. Qi, S. Luo, C. Au, Synthesis of magnetic ion-imprinted fluorescent CdTe quantum dots by chemical etching and their visualization application for selective removal of Cd(II) from water, *Colloids Surf., A: Physicochem. Eng. Aspects* 462 (2014) 186–193.
- [16] Q. Sun, S. Fu, T. Dong, S. Liu, C. Huang, Aqueous synthesis and characterization of TGA-capped CdSe quantum dots at freezing temperature, *Molecules* 17 (2012) 8430–8438.
- [17] D. Sukanya, P. Sagayaraj, Facile synthesis and characterization of MPA capped CdSe and CdSe/ZnS

- nanocrystals, *Int. J. Chem. Tech. Res.* 7 (2014–2015) 1421–1425.
- [18] P. Kumar, D. Kukkar, A. Deep, S.C. Sharma, L.M. Bharadwaj, Synthesis of mercaptopropionic acid stabilized CdS quantum dots for bioimaging in breast cancer, *Adv. Mater. Lett.* 3 (2012) 471–475.
- [19] N.A. Hamizi, C.S. Ying, M.R. Johan, Synthesis with different Se concentrations and optical studies of CdSe quantum dots via inverse micelle technique, *Int. J. Electrochem. Sci.* 7 (2012) 4727–4734.
- [20] J. Tauc, A. Menth, States in the gap, *J. Non-Cryst. Solids* 8–10 (1972) 569–585.
- [21] N.M. Mahmoodi, M. Arami, N.Y. Limaee, N.S. Tabrizi, Kinetics of heterogeneous photocatalytic degradation of reactive dyes in an immobilized TiO₂ photocatalytic reactor, *J. Colloid Interface Sci.* 295 (2006) 159–164.
- [22] N.M. Mahmoodi, Binary catalyst system dye degradation using photocatalysis, *Fibers Polym.* 15 (2014) 273–280.